Editors' Suggestion

Oxygen Quadclusters in SiO_2 Glass above Megabar Pressures up to 160 GPa revealed by X-ray Raman Scattering

Sung Keun Lee,[1,2,*] Yong-Hyun Kim,[1] Yoo Soo Yi,[1] Paul Chow,[3] Yuming Xiao,[3] Cheng Ji,[4] and Guoyin Shen[3,†]

[1]School of Earth and Environmental Sciences, Seoul National University, Seoul 08826, Korea
[2]Institute of Applied Physics, Seoul National University, Seoul 08826, Korea
[3]HPCAT, X-Ray Science Division, Argonne National Laboratory, Argonne, Illinois 60439, USA
[4]Geophysical Laboratory, Carnegie Institution for Science, Argonne, Illinois 60439, USA

(Received 13 July 2019; published 5 December 2019)

As oxygen may occupy a major volume of oxides, a densification of amorphous oxides under extreme compression is dominated by reorganization of oxygen during compression. X-ray Raman scattering (XRS) spectra for SiO_2 glass up to 1.6 Mbar reveal the evolution of heavily contracted oxygen environments characterized by a decrease in average O-O distance and the potential emergence of quadruply coordinated oxygen (oxygen quadcluster). Our results also reveal that the edge energies at the centers of gravity of the XRS features increase *linearly* with bulk density, yielding the first predictive relationship between the density and partial density of state of oxides above megabar pressures. The extreme densification paths with densified oxygen in amorphous oxides shed light upon the possible existence of stable melts in the planetary interiors.

DOI: 10.1103/PhysRevLett.123.235701

Compressed glasses that undergo densification *far above* megabar pressures (i.e., pressures above 100 GPa) may consist of heavily entangled amorphous structures that are different from those at lower pressures, as well as from those observed in crystalline analogs. While the structures of major crystals in Earth's mantle at pressures greater than 100 GPa are well understood, the atomic configurations of noncrystalline silicates at the bottom of the mantle at pressures of ~130 GPa remain unclear due to experimental difficulties [1,2]. Furthermore, considering much larger radii of the super Earths, the silicate parts in those planetary bodies are extended into much higher pressure conditions. Detailed structures of silicate melts at pressure conditions much higher than that of Earth's lower mantle remain elusive.

Known as the prototypical amorphous oxide, SiO_2 glass (a-SiO_2) may give rise to a diverse roster of bonding configurations when compressed beyond megabar pressures. a-SiO_2 is also a major component of technologically important oxide glasses and yields atomistic insight into the differentiation of the primitive mantle from the magma ocean and the evolution of super Earths [3]. The structural changes in a-SiO_2 at high pressures provide simplified yet essential densification paths for complex silicates, including SiO_2-rich melts at the bottom of Earth's mantle and that of other super-Earth bodies [2–6] and are responsible for the anomalous pressure dependence of the elastic properties of a-SiO_2 under compression [7].

Densification in silicates has traditionally been described in terms of how cations are rearranged under compression (e.g., the Si coordination number) [8–10]. However, in a simplified model of ionic oxide, considering its much larger ionic radius, oxygen (with an ionic radius of ~1.4 Å, compared to 0.28 Å for Si)—the most abundant element in bulk silicate Earth—occupies a major volume of oxides. The degree of oxide densification at high pressures is likely to be dominated by the reorganization of oxygen during compression [see Sec. 1 of the Supplemental Material (SM) [11]]. While the nature of oxygen in a-SiO_2 undergoing densification is enigmatic, the average Si coordination number of a-SiO_2 increases with increasing pressure, forming highly coordinated Si ($^{[5,6]}$Si) (see Refs. [3,7,10,40–42] and Sec. 2 of the SM [11]). The formation of $^{[5,6]}$Si in a-SiO_2 is accompanied by the formation of *triply* coordinated oxygen ($^{[3]}$O, oxygen triclusters) [43] from *doubly* coordinated bridging oxygen ($^{[4]}$Si–$^{[2]}$O–$^{[4]}$Si; see Sec. 1 of the SM [11]). Elastic x-ray scattering measurements of a-SiO_2 have indicated that the average coordination number of Si may be larger than 6 near 100 GPa, reaching up to ~6.9 at 170 GPa (see Ref. [41] and Fig. S1 in the SM [11]). This implies that, in addition to $^{[3]}$O, other highly coordinated oxygen may form above 1.2 Mbar pressures. The potential presence and the electronic structures of oxygen beyond $^{[3]}$O in amorphous oxides need to be confirmed. Information regarding oxygen-specific changes occurring under compression will resolve the puzzle of the glass structure under well-beyond-megabar pressures, constraining the densification mechanisms of amorphous oxides.

Despite their importance, previous efforts to identify the direct *oxygen-specific* configurations of a-SiO_2 and silicate

glasses well above megabar pressures have remained challenging (see Sec. 2 of the SM [11]). X-ray Raman scattering (XRS) reveals local electronic bonding environments around oxygen in diverse oxides through the partial electronic density of states (PDOS) [43–49]. Key to the successful application of XRS studies under megabar pressure conditions is the efficient capture of inelastically scattered photons from compressed samples while the background signals from the gaskets used to sustain high-pressure conditions are minimized [50,51]. However, the XRS process is inefficient, as it yields signal intensity that is 3–6 orders of magnitude smaller than that of elastic x rays (see Sec. 3 of the SM [11]). Recent advances in the postcollimation of inelastically scattered x rays shed light on an opportunity to collect high-resolution XRS signals under extreme compression [46], while the inherent inefficiency limits the maximum pressure conditions for the collection of inelastic scattering x rays of any condensed matter to ~120 GPa. In this Letter, the experimental breakthrough allows us to collect the XRS signal of contracted oxygen in a-SiO_2 well above megabar pressures up to 160 GPa. We provide spectroscopic proxies based on O K-edge XRS from which to infer the densification of silicate melts far beyond megabar pressures.

The a-SiO_2 (Corning FS7980) was loaded into a panoramic diamond anvil cell using a beryllium gasket (see Sec. 4 of the SM [11] for detailed experimental conditions and Ref. [46]). The diamond culet for the experiment up to 124 GPa is 150 μm, and that at higher pressures up to 160 GPa is 110 μm. The Be gasket was preindented with a hole diameter of ~40–60 μm. Oxygen K-edge XRS spectra for the a-SiO_2 were collected at the HPCAT beam line 16-ID-D at the Advanced Photon Source. The XRS spectra were collected by scanning the incident photon energy relative to the analyzer energy of 9.908 keV. The incident x rays were produced by a double-crystal Si(111) monochromator. Kirkpatrick-Baez mirrors and a pinhole upstream of the sample focus a beam with a FWHM of 8 (horizontal) × 5 (vertical) μm^2. A polycapillary (PC) postcollimation optics was combined with a single spherical Si(555) analyzer, with an Amptek silicon detector. A PC with a 7 mm working distance and a collection cone angle of 12° was employed [46,50], making the scattering angle vary from 19° to 31°. The Raman signal from the diamond culet was used to estimate the pressure [52]. The pressure variation within the sample chamber at high-pressure conditions is up to ~10 GPa (see Sec. 4 of the SM [11]). The spectra were collected from 1 atm to 160 GPa, with energy loss (incident energy-elastic energy) varying from 530 to 565 eV.

The oxygen K-edge XRS spectra for a-SiO_2 at high pressures up to 160 GPa exhibit a series of pressure-induced changes in edge features centered at ~538, ~544, and ~548 eV (see Fig. 1 and Sec. 5 of the SM [11]), revealing dramatic changes in the oxygen environments

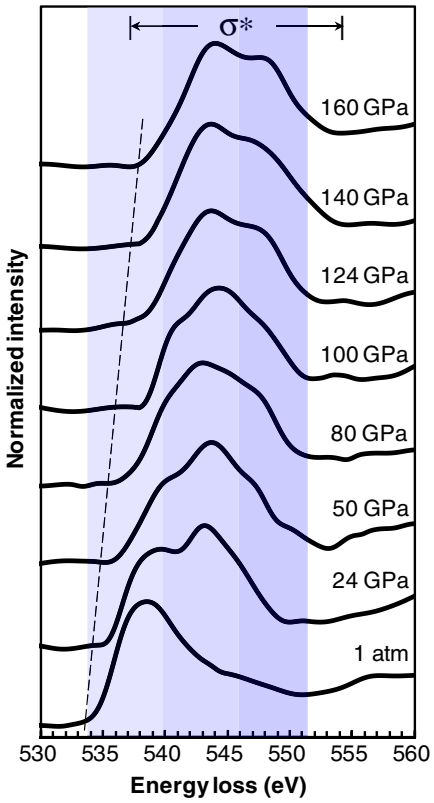

FIG. 1. Oxygen K-edge XRS spectra of SiO_2 glass at pressures up to ~160 GPa plotted as the normalized scattered photon intensity vs the energy loss (incident energy-elastic energy). See Fig. S2 in the SM [11] for the XRS spectra without smoothing in accordance with the spectral uncertainty.

under compression. The spectrum at 1 atm shows a broad peak at 538 eV that represents the transition of a core electron to a σ^* antibonding $2p$ state in $^{[2]}$O coordinated with two $^{[4]}$Si frameworks (see Sec. 6 of the SM [11]). The spectrum also shows a minor shoulder at ~545 eV, which is consistent with an earlier O K-edge XRS spectrum [43,48]. The main σ^* peak shifts to high energy with increasing pressure. At pressures of ~24 GPa, a major spectral feature at ~544 to 545 eV appears, with its intensity increasing as pressure increases up to ~80 GPa. The systematic increase in the absorption threshold (the dotted line in Fig. 1) corresponds to a decrease in the average O-O distance ($d_{O\text{-}O}$) (see Refs. [53,54] and Sec. 6 of the SM [11]). Furthermore, the fraction of $^{[3]}$O gradually increases as pressure increases, similar to the results from *ab initio* MD simulations of a-SiO_2 (see Ref. [55] and Sec. 2 of the SM [11]). Thus, the formation of $^{[3]}$O and the variations in the short-to-medium-range structures accompanying the growth of $^{[3]}$O contribute to the feature at ~544 eV [44].

The XRS spectrum at 100 GPa reveals the emergence of an additional feature at ~548 eV. Its intensity is more prominent in the spectrum at 124 GPa. With a further increase in pressure, the spectra collected at 140 and

160 GPa revealed an increase in high energy features. This feature indicates that an additional densification of amorphous networks other than the formation of $^{[3]}$O may prevail above megabar pressures. The O K-edge XRS features could be due to diverse structural changes associated with the densification (see Sec. 6 of the SM [11]): as the average coordination number of Si in this pressure range is larger than 6 (see Sec. 2 of the SM [11]), this feature indicates the evolution of oxygen configurations involving quadruply coordinated oxygen ($^{[4]}$O, oxygen quadclusters) and a significant reduction in oxygen proximity. Multiple structural arrangements around $^{[4]}$O resulting from the distribution of $^{[5,6,7]}$Si around the highly coordinated oxygen explain the features observed at 548 eV. The K-edge features at higher pressures are also broader than those at 1 atm, indicating an increase in dispersion in the O-2p and O-d PDOS of the compressed oxygen [53,54]. This dispersion results from more complex atomic configurations [e.g., $^{[3,4]}$O with varying Si coordination states ($^{[5,6,7]}$Si)] around the oxygen and wider O-O distribution at high pressures. The distortion of Si polyhedra involving $^{[4]}$O and, thus, the Si-O bond-length distribution is likely to be more prominent well above megabar pressures [56]. This indicates that the extent of structural disorder in a-SiO_2 increases above megabar pressures. Because melt viscosity at high pressures decreases with the increasing configurational entropy of melts [57], the pressure-induced changes in structural disorder associated with the emergence of $^{[4]}$O suggest a decrease in melt viscosity at the bottom of the mantle.

To elaborate on the oxygen environments in a-SiO_2 under extreme compression, the O K-edge XRS spectra for a-SiO_2 are compared with those calculated for crystalline phases (Fig. 2 and Fig. S3 in Sec. 7 of the SM [11]; the simulation methods are presented in Sec. 7 of the SM [11]). With increasing pressure, crystalline SiO_2 undergoes phase transitions from quartz (1 atm) and stishovite (~ 9.3 GPa) to higher-pressure phases, including α-PbO_2 type at $\sim$120 GPa [58–61]. The edge features and the absorption threshold for these crystalline phases both shift to higher energy ($\sim$4 to 5 eV) as the pressure increases up to 120 GPa, which is consistent with the trend observed for $MgSiO_3$ phases [53,54]. The main peak at 538 eV for quartz is similar to that for a-SiO_2 at 1 atm. The doubletlike feature at $\sim$536 and 543 eV in stishovite at 29 GPa is characteristic of $^{[3]}$O linking three $^{[6]}$Si atoms in an edge-sharing topology [53,54], similar to the features for a-SiO_2 at 24 GPa (Fig. 1). The calculated spectrum for the α-PbO_2 phase at 120 GPa reveals a feature at 546–548 eV, indicating a further reduction in average $d_{\text{O-O}}$ (see Sec. 8 of the SM [11]).

The observed changes in the O K-edge features for the crystalline phases and a-SiO_2 reveal the structural adaptation of the oxides upon densification. In particular, the edge energies at the centers of gravity (E_c) of the main σ^*

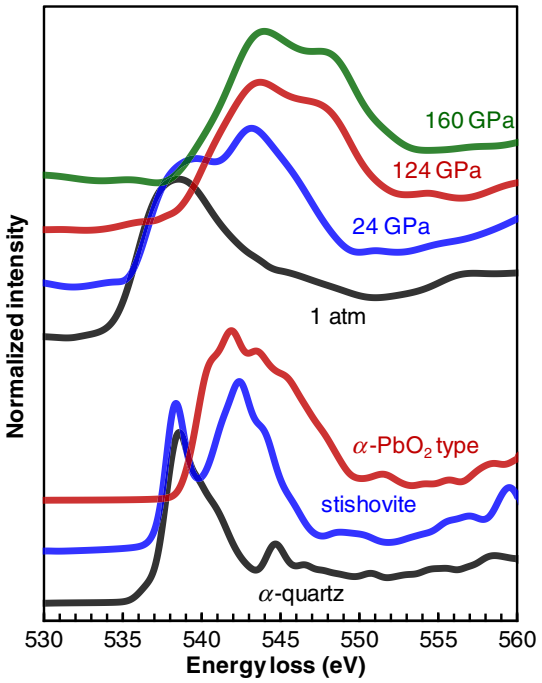

FIG. 2. Calculated oxygen K-edge XRS spectra for α-quartz (1 atm), stishovite ($\sim$29.1 GPa), and α-PbO_2-type SiO_2 ($\sim$120 GPa) with the Gaussian broadening factor of 1 eV (see Sec. 7 of the SM [11] for the calculation methods). The K-edge XRS spectra of a-SiO_2 under similar pressure conditions and that at 160 GPa are shown for comparison.

features of the diverse crystalline phases and a-SiO_2 increase upon compression [see Fig. 3(a), Figs. S4 and S5 in the SM [11], and, for the calculation of E_c, Sec. 9 of the SM [11]]. Because the average $d_{\text{O-O}}$ values in crystalline silica systematically decrease with pressure (Tables S1 and S2 in the SM [11]), the E_c increases with a decreasing average $d_{\text{O-O}}$ [i.e., $E_c(\text{eV}) \approx -13.1 \times d_{\text{O-O}} + 575.5$] [Fig. 3(b)]. Therefore, E_c can be regarded as a measure of oxygen proximity for oxide densification under extreme compression at *beyond*-megabar pressures. Based on the trend, an observed shift in the σ^* peak in a-SiO_2 corresponds to a decrease in $d_{\text{O-O}}$ of $\sim$0.35 Å at pressures up to $\sim$124 GPa, which is comparable to the estimated decrease due to densification (and an increase in the oxygen packing density) in the crystalline phases ($\sim$0.3 Å) [the difference between the $d_{\text{O-O}}$ of quartz (2.6261 Å) and that of α-PbO_2 (2.3273 Å)] [9] (see Sec. 7 and Table S2 in the SM [11]). We also found that the increase in E_c is well correlated with the increase in the bulk density (ρ) of a-SiO_2 [Fig. 3(c)]. Here, we used the density of a-SiO_2 as obtained from a pioneering x-ray absorption study [62]. As the E_c values depend on the way in which the peak positions were determined (see Sec. 9 of the SM [11]), the results provide a semiquantitative trend. Nevertheless, the relationship can be described by the following linear equation, $E_c(\text{eV}) \approx 1.6 \times \rho + 536.6$, revealing the predictive relationship between the glass

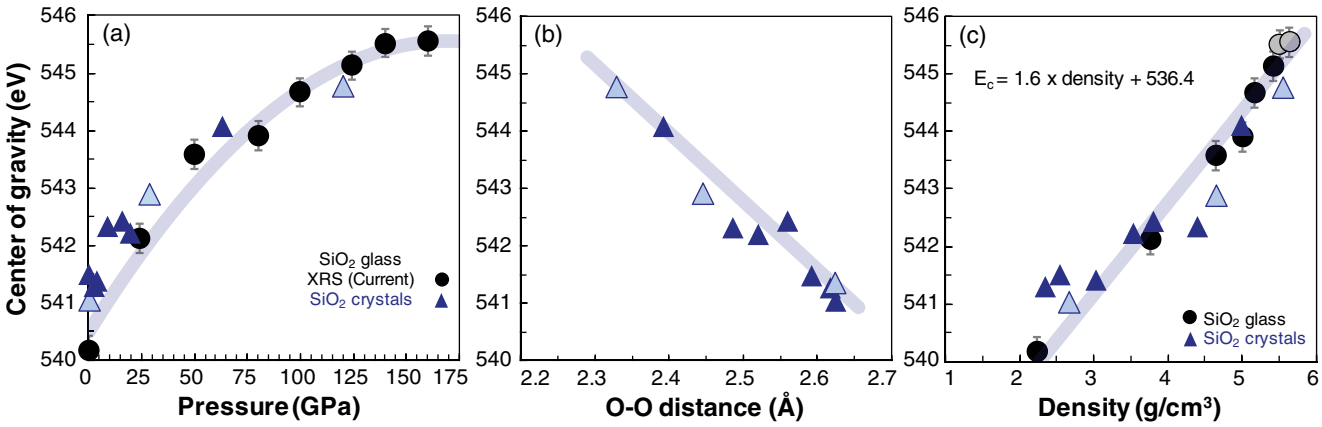

FIG. 3. (a) Variation of the edge energy at the center of gravity (E_c) in the oxygen K-edge XRS spectrum for a-SiO_2 (black circles) with varying pressure. The E_c values for crystalline silica polymorphs are also shown (blue triangles). The pale blue symbols are based on the three polymorphs shown in Fig. 2 (see Sec. 7 of the SM [11]). (b) E_c values of crystalline SiO_2 phases with varying O-O distances. (c) Relationship between E_c and density for crystalline and amorphous SiO_2. The densities of the a-SiO_2 glasses were from a recent experiment [62].

density and the partial density of state of oxides above megabar pressures. The current results establish the first simple relationship between the density, the oxygen proximity (i.e., $d_{O\text{-}O}$), and a shift in the O K-edge energy (parametrized by E_c). Both the oxygen proximity and E_c (the experimentally measurable quantity) can be used as novel proxies for the densification of oxides at high pressures up to 160 GPa.

The average Si coordination number (C_{Si}) in a-SiO_2 increases from 4 to 6 with increasing pressure up to ~100 GPa [10,40,42]. C_{Si} is greater than 6 at high pressures above ~100 GPa, forming $^{[7]}$Si (see Sec. 2 of the SM [11] and Ref. [41]). Considering the relationship between the cation coordination number and the average oxygen coordination number (C_O) in a-SiO_2, i.e., $C_{Si} = 2 \times C_O$ [63–65], the C_O in a-SiO_2 above megabar pressures is larger than 3. Figure 4 shows the average oxygen coordination number values calculated from the average Si coordination number from experimental studies (see Refs. [40–42,66] and Sec. 2 of the SM [11]). Formation of oxygen triclusters ($3^{[5,6]}$Si-$^{[3]}$O) in a-SiO_2 below 100 GPa results from a pressure-induced chemical bonding between $^{[2]}$O and $^{[4,5]}$Si. Above megabar pressures, oxygen quadclusters (e.g., $4^{[6,7]}$Si-$^{[4]}$O) form through the annihilation of $^{[3]}$O and $^{[6]}$Si (e.g., $3^{[6]}$Si-$^{[3]}$O + $^{[6]}$Si → $4^{[6,7]}$Si-$^{[4]}$O), and the fraction of $^{[4]}$O is expected to gradually increase as pressure increases. At ~120 GPa, considering the estimated C_O value of 3.25 [41] (assuming the presence only of $^{[3,4]}$O above megabar pressures, and thus the absence of $^{[2]}$O), ~75% of the oxygen exists in the form of $^{[3]}$O, while ~25% of the oxygen is present as $^{[4]}$O (i.e., $0.25 \times 4 + 0.75 \times 3 = 3.25$). Furthermore, at ~160 GPa, the C_O value can be ~3.4 [41]. Then, ~60% of the oxygen exists in the form of $^{[3]}$O, while ~40% of the oxygen is present as $^{[4]}$O (i.e., $0.4 \times 4 + 0.6 \times 3 = 3.4$). The changes in the O K-edge XRS features in a-SiO_2 and E_c are well correlated with C_O, and spectral evolutions up to 1.6 Mbar pressures may indicate the formation of $^{[4]}$O [56]. As the C_{Si} from the theoretical calculations is somewhat lower [7,56], a quantitative fraction of $^{[4]}$O remains to be confirmed

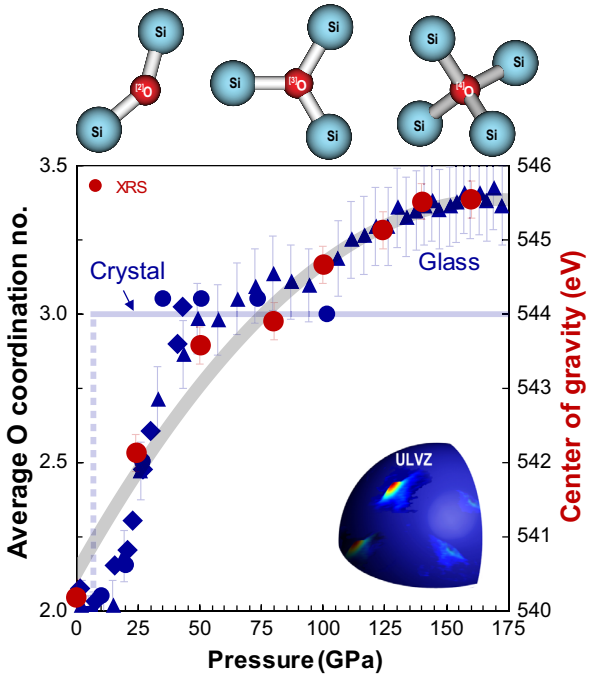

FIG. 4. Changes in the *average* oxygen coordination number (C_O) and E_c of SiO_2 glass up to 160 GPa. The C_O values are calculated from the average silicon coordination numbers (C_{Si}) from previous studies [blue circle [42]; blue diamond [40]; blue triangle [41]; red circle (this Letter), based on E_c in Fig. 3; see Sec. 2 of the SM [11]]. Schematics of the oxygen configurations with varying coordination numbers (top) and ultralow velocity zone (ULVZ) at the lower mantle are shown.

(Sec. 2 of the SM [11]). A complementary view of the oxygen coordination transformation in oxides was provided in an earlier model from O'Keeffe and Hyde [67–69], where the changes in electronic structures around oxygen upon compression are determined by varying numbers of the nearest neighbor Si. The hindrance to form highly coordinated oxygen stems from the repulsive Si…Si interactions. The degree of densification can be described by the distance between the Si's, while $d_{O\text{-}O}$ was used to describe the densification in amorphous oxides in the current Letter. The linear relationship between oxygen PDOS and the bulk density indicates a collective nature of the oxygen PDOS that reflects short-to-intermediate-range configurations around oxygen [53,54]. A low-energy vibrational density of states also correlates well with the density of a-SiO_2 because of its collective nature [70].

The current experimental breakthroughs with oxygen-specific XRS spectra for a-SiO_2 up to 1.6 Mbar allow us to draw conclusions regarding the oxygen bonding nature in amorphous oxides under compression that differ from those of crystals. Densification in crystalline silica under compression is achieved through changes in long-range topological rearrangements upon phase transition without coordination transformation up to 160 GPa. For example, the α-PbO_2 phase has coordination environments similar to those of lower-pressure phases (the $CaCl_2$-type phase and stishovite): all of these phases consist of $^{[6]}$Si and $^{[3]}$O. In contrast, densification in a-SiO_2 results in gradual changes in short-range configurations and the formation of more highly coordinated configurations, including $^{[7]}$Si and $^{[4]}$O, above megabar pressures up to 160 GPa. The oxygen-specific densification path is characterized by the formation of oxygen quadclusters, making the $^{[4]}$O fraction a new indicator of melt densification.

The behavior of a-SiO_2 under compression gives clues about how densification occurs for noncrystalline silicates on Earth and in planetary interiors. Note that the dense partial melts have additional components, such as MgO, FeO, and H_2O [71–73]. In such melts, the formation of highly coordinated oxygen becomes more complex, as average Si and oxygen coordination numbers of Mg-rich melts are smaller than those of SiO_2 liquids (see Refs. [74,75] and Sec. 1 of the SM [11]). Further experimental efforts for complex silicate melts at an elevated temperature conditions are required. Nevertheless, along with the silica-rich nature of the proposed partial melts in the ultralow velocity zone (ULVZ) [4], the current densification model for a-SiO_2 can be applied to account for the unusual stability and structural transformation in complex melts at the core mantle boundary (CMB) [76], as SiO_2 is a major end-member of any magma composition. Densified deep mantle melts consisting primarily of $^{[3,4]}$O configurations result in enhanced topological contraction, providing a potential path for extreme melt densification at the CMB and the negative buoyancy of such melts in deep magma ocean and that in the super Earths.

Finally, while O K-edge XRS is a unique probe of the electronic density of states of crystalline and amorphous materials at high pressure, the pressure-induced changes in the spectra up to ~50 GPa are subtle, so the full utility of the XRS technique has not often been demonstrated in previous applications. The current study of silica at pressures up to 160 GPa shows that the XRS spectrum changes drastically with extreme compression, so this technique is suitable for use in studying the detailed bonding under compression at beyond-megabar pressures. The conceptual advances (i.e., oxygen-specific densification mechanism, electronic density of state vs bulk density above megabar pressure conditions) and experimental breakthroughs allow us to account for the densification in an enormous number of glass-forming oxides. Despite the unsurmountable challenges that lie ahead for XRS techniques, the current results offer inspiration for the application of XRS studies of complex glasses, as well as crystals under multimegabar pressure conditions.

We thank three anonymous reviewers for constructive suggestions which improved the manuscript's quality. This work was supported by the National Research Foundation, Korea (Grant No. 2017R1A2A1A17069511) and the Samsung Science and Technology Foundation (SSTF) (Grant No. BA1401-07) to S. K. L., G. S. acknowledges the support from the U.S. DOE-BES, Division of Materials Sciences and Engineering, under Award No. DE-FG02-99ER45775. HPCAT operations are supported by the DOE-NNSA's Office of Experimental Sciences. The Advanced Photon Source is a user facility operated for the DOE Office of Science by Argonne National Laboratory under Contract No. DE-AC02-06CH11357.

*Corresponding author.
sungklee@snu.ac.kr
†Corresponding author.
gyshen@anl.gov

[1] R. J. Hemley, V. V. Struzhkin, R. E. Cohen, and G. Shen, in *Treatise on Geophysics*, 2nd ed., edited by G. Schubert (Elsevier, Oxford, 2015), p. 313.
[2] T. Lay, in *Treatise on Geophysics*, 2nd ed., edited by G. Schubert (Elsevier, Oxford, 2015), p. 683.
[3] B. B. Karki, D. Bhattarai, and L. Stixrude, Phys. Rev. B **76**, 104205 (2007).
[4] D. Andrault, G. Pesce, M. A. Bouhifd, B. N. Casanova, J. M. Hénot, and M. Mezouar, Science **344**, 892 (2014).
[5] M. Murakami and J. D. Bass, Phys. Rev. Lett. **104**, 025504 (2010).
[6] R. Scipioni, L. Stixrude, and M. P. Desjarlais, Proc. Natl. Acad. Sci. U.S.A. **114**, 9009 (2017).
[7] M. Wu, Y. Liang, J.-Z. Jiang, and J. S. Tse, Sci. Rep. **2**, 398 (2012).

[8] Y. Wang, T. Sakamaki, L. B. Skinner, Z. Jing, T. Yu, Y. Kono, C. Park, G. Shen, M. L. Rivers, and S. R. Sutton, Nat. Commun. **5**, 3241 (2014).

[9] A. Zeidler, P. S. Salmon, and L. B. Skinner, Proc. Natl. Acad. Sci. U.S.A. **111**, 10045 (2014).

[10] A. Zeidler *et al.*, Phys. Rev. Lett. **113**, 135501 (2014).

[11] See Supplemental Material at http://link.aps.org/supplemental/10.1103/PhysRevLett.123.235701, which includes Refs. [12–39], for the summary of the earlier studies on the SiO_2 and other silicate glasses, additional details on the experimental and computational methods, summary of the earlier XRS studies for oxide crystals and glasses at high pressure, and estimation of center of gravity of the O *K*-edge XRS spectra.

[12] J. R. Allwardt, J. F. Stebbins, B. C. Schmidt, D. J. Frost, A. C. Withers, and M. M. Hirschmann, Am. Mineral. **90**, 1218 (2005).

[13] S. K. Lee, Solid State Nucl. Magn. Reson. **38**, 45 (2010).

[14] S. K. Lee, G. D. Cody, Y. W. Fei, and B. O. Mysen, Geochim. Cosmochim. Acta **68**, 4189 (2004).

[15] S. K. Lee, Y. S. Yi, G. D. Cody, K. Mibe, Y. W. Fei, and B. O. Mysen, J. Phys. Chem. C **116**, 2183 (2012).

[16] X. Xue, J. F. Stebbins, and M. Kanzaki, Am. Mineral. **79**, 31 (1994).

[17] J. L. Yarger, K. H. Smith, R. A. Nieman, J. Diefenbacher, G. H. Wolf, B. T. Poe, and P. F. McMillan, Science **270**, 1964 (1995).

[18] G. H. Wolf and P. F. McMillan, in *Structure, Dynamics, and Properties of Silicate Melts*, edited by J. F. Stebbins, P. F. McMillan, and D. B. Dingwell (Mineralogical Society of America, Washington, DC, 1995), p. 505.

[19] J.-L. Barrat, J. Badro, and P. Gillet, Mol. Simul. **20**, 17 (1997).

[20] J. S. Tse, D. D. Klug, and Y. Le Page, Phys. Rev. B **46**, 5933 (1992).

[21] A. Zeidler *et al.*, Phys. Rev. B **90**, 024206 (2014).

[22] S. K. Lee, J. Phys. Chem. B **108**, 5889 (2004).

[23] J. F. Stebbins, Am. Mineral. **101**, 753 (2016).

[24] J. F. Stebbins and X. Y. Xue, in *Spectroscopic Methods in Mineralology and Materials Sciences*, edited by G. S. Henderson, D. R. Neuville, and R. T. Downs (Mineralogical Society of America, Washington, DC, 2014), p. 605.

[25] S. K. Lee, K. Mibe, Y. W. Fei, G. D. Cody, and B. O. Mysen, Phys. Rev. Lett. **94**, 165507 (2005).

[26] W. L. Mao *et al.*, Science **302**, 425 (2003).

[27] Y. Meng, P. J. Eng, J. S. Tse, D. M. Shaw, M. Y. Hu, J. Shu, S. A. Gramsch, C.-c. Kao, R. J. Hemley, and H.-k. Mao, Proc. Natl. Acad. Sci. U.S.A. **105**, 11640 (2008).

[28] B. J. A. Moulton, G. S. Henderson, H. Fukui, N. Hiraoka, D. de Ligny, C. Sonneville, and M. Kanzaki, Geochim. Cosmochim. Acta **178**, 41 (2016).

[29] W. Schulke, in *Electron Dynamics by Inelastic X-Ray Scattering* (Oxford University Press New York, 2007), p. 186.

[30] Y. Lin, L. Zhang, H.-k. Mao, P. Chow, Y. Xiao, M. Baldini, J. Shu, and W. L. Mao, Phys. Rev. Lett. **107**, 175504 (2011).

[31] H. Fukui, M. Kanzaki, N. Hiraoka, and Y. Q. Cai, Phys. Chem. Miner. **36**, 171 (2009).

[32] S. K. Lee, P. J. Eng, H. K. Mao, Y. Meng, and J. Shu, Phys. Rev. Lett. **98**, 105502 (2007).

[33] S. K. Lee, P. J. Eng, H. K. Mao, and J. F. Shu, Phys. Rev. B **78**, 214203 (2008).

[34] S. K. Lee, S. Y. Park, H. I. Kim, O. Tschauner, P. Asimow, L. Bai, Y. Xiao, and P. Chow, Geophys. Res. Lett. **39**, L05306 (2012).

[35] P. Blaha, K. Schwarz, G. K. H. Madsen, D. Kvasnicka, J. Luitz, R. Laskowski, F. Tran, and L. D. Marks, *WIEN2k, An Augmented Plane Wave + Local Orbitals Program for Calculating Crystal Properties* (Karlheinz Schwarz, Techn. Universität Wien, Austria, 2018).

[36] J. P. Perdew, A. Ruzsinszky, G. I. Csonka, O. A. Vydrov, G. E. Scuseria, L. A. Constantin, X. Zhou, and K. Burke, Phys. Rev. Lett. **100**, 136406 (2008).

[37] G. Will, M. Bellotto, W. Parrish, and M. Hart, J. Appl. Crystallogr. **21**, 182 (1988).

[38] T. Yamanaka, T. Fukuda, and J. Mimaki, Phys. Chem. Miner. **29**, 633 (2002).

[39] D. M. Teter, R. J. Hemley, G. Kresse, and J. Hafner, Phys. Rev. Lett. **80**, 2145 (1998).

[40] C. J. Benmore, E. Soignard, S. A. Amin, M. Guthrie, S. D. Shastri, P. L. Lee, and J. L. Yarger, Phys. Rev. B **81**, 054105 (2010).

[41] C. Prescher, V. B. Prakapenka, J. Stefanski, S. Jahn, L. B. Skinner, and Y. Wang, Proc. Natl. Acad. Sci. U.S.A. **114**, 10041 (2017).

[42] T. Sato and N. Funamori, Phys. Rev. B **82**, 184102 (2010).

[43] S. K. Lee *et al.*, Proc. Natl. Acad. Sci. U.S.A. **105**, 7925 (2008).

[44] S. K. Lee, P. J. Eng, and H. K. Mao, in *Spectroscopic Methods in Mineralogy and Materials Sciences*, edited by G. S. Henderson, D. R. Neuville, and R. T. Downs (Mineralogical Society of America, Washington, DC, 2014), p. 139.

[45] S. K. Lee, P. J. Eng, H. K. Mao, Y. Meng, M. Newville, M. Y. Hu, and J. F. Shu, Nat. Mater. **4**, 851 (2005).

[46] S. K. Lee, Y.-H. Kim, P. Chow, Y. Xiao, C. Ji, and G. Shen, Proc. Natl. Acad. Sci. U.S.A. **115**, 5855 (2018).

[47] G. Lelong, L. Cormier, G. Ferlat, V. Giordano, G. S. Henderson, A. Shukla, and G. Calas, Phys. Rev. B **85**, 134202 (2012).

[48] J. F. Lin *et al.*, Phys. Rev. B **75**, 012201 (2007).

[49] C. Sternemann and M. Wilke, High Press. Res. **36**, 275 (2016).

[50] P. Chow, Y. M. Xiao, E. Rod, L. G. Bai, G. Y. Shen, S. Sinogeikin, N. Gao, Y. Ding, and H.-K. Mao, Rev. Sci. Instrum. **86**, 072203 (2015).

[51] S. Petitgirard *et al.*, Geochem. Perspect. Lett. **9**, 32 (2019).

[52] Y. Akahama and H. Kawamura, High Press. Res. **27**, 473 (2007).

[53] Y. S. Yi and S. K. Lee, Am. Mineral. **97**, 897 (2012).

[54] Y. S. Yi and S. K. Lee, Phys. Rev. B **94**, 094110 (2016).

[55] A. Trave, P. Tangney, S. Scandolo, A. Pasquarello, and R. Car, Phys. Rev. Lett. **89**, 245504 (2002).

[56] M. Murakami, S. Kohara, N. Kitamura, J. Akola, H. Inoue *et al.*, Phys. Rev. B **99**, 045153 (2019).

[57] S. K. Lee, Proc. Natl. Acad. Sci. U.S.A. **108**, 6847 (2011).

[58] R. E. Cohen, in *High-Pressure Research: Application to Earth, and Planetary Sciences*, edited by Y. Syono and

M. H. Manghnani (Terra Scientific Publishing Company, Tokyo, 1992), p. 425.
[59] B. B. Karki, L. Stixrude, and J. Crain, Geophys. Res. Lett. **24**, 3269 (1997).
[60] M. Murakami, K. Hirose, S. Ono, and Y. Ohishi, Geophys. Res. Lett. **30**, 1207 (2003).
[61] T. Tsuchiya, R. Caracas, and J. Tsuchiya, Geophys. Res. Lett. **31**, L11610 (2004).
[62] S. Petitgirard *et al.*, Phys. Rev. Lett. **119**, 215701 (2017).
[63] S. K. Lee and E. J. Kim, J. Phys. Chem. C **119**, 748 (2015).
[64] S.-Y. Xie, L. Wang, F. Liu, X.-B. Li, L. Bai, V. B. Prakapenka, Z. Cai, H.-k. Mao, S. Zhang, and H. Liu, J. Phys. Chem. Lett. **9**, 2388 (2018).
[65] S. K. Lee and S. Ryu, J. Phys. Chem. Lett. **9**, 150 (2018).
[66] T. Sato and N. Funamori, Phys. Rev. Lett. **101**, 255502 (2008).
[67] M. O'Keeffe and B. G. Hyde, Nature (London) **309**, 411 (1984).
[68] M. O'Keeffe and B. G. Hyde, in *Structure and Bonding in Crystals*, edited by M. O'Keeffe and A. Navrotsky (Academic Press, New York, 1981), p. 227.
[69] M. O'Keeffe and B. G. Hyde, J. Solid State Chem. **44**, 24 (1982).
[70] A. I. Chumakov, G. Monaco, A. Fontana, A. Bosak, R. P. Hermann *et al.*, Phys. Rev. Lett. **112**, 025502 (2014).
[71] E. Ohtani, Chem. Geol. **418**, 6 (2015).
[72] Y. F. Duan, N. Y. Sun, S. H. Wang, X. Y. Li, X. Guo, H. W. Ni, V. B. Prakapenka, and Z. Mao, Earth Planet. Sci. Lett. **494**, 92 (2018).
[73] J. Liu *et al.*, Nature (London) **551**, 494 (2017).
[74] D. B. Ghosh, B. B. Karki, and L. Stixrude, Am. Mineral. **99**, 1304 (2014).
[75] L. Stixrude and B. Karki, Science **310**, 297 (2005).
[76] I. Ohira, M. Murakami, S. Kohara, K. Ohara, and E. Ohtani, Prog. Earth Planet. Sci. **3**, 18 (2016).